Regulation of *Chlamydomonas* flagella and ependymal cell motile cilia by ceramide-mediated translocation of GSK3

Ji Na Kong[a], Kara Hardin[a], Michael Dinkins[a], Guanghu Wang[a], Qian He[a], Tarik Mujadzic[a], Gu Zhu[a], Jacek Bielawski[b], Stefka Spassieva[c], and Erhard Bieberich[a]

[a]Department of Neuroscience and Regenerative Medicine, Medical College of Georgia, Georgia Regents University, Augusta, GA 30912; [b]Department of Biochemistry and Molecular Biology and [c]Department of Medicine, Medical University of South Carolina, Charleston, SC 29425

ABSTRACT **Cilia are important organelles formed by cell membrane protrusions; however, little is known about their regulation by membrane lipids. We characterize a novel activation mechanism for glycogen synthase kinase-3 (GSK3) by the sphingolipids phytoceramide and ceramide that is critical for ciliogenesis in *Chlamydomonas* and murine ependymal cells, respectively. We show for the first time that *Chlamydomonas* expresses serine palmitoyl transferase (SPT), the first enzyme in (phyto)ceramide biosynthesis. Inhibition of SPT in *Chlamydomonas* by myriocin led to loss of flagella and reduced tubulin acetylation, which was prevented by supplementation with the precursor dihydrosphingosine. Immunocytochemistry showed that (phyto)ceramide was colocalized with phospho–Tyr-216-GSK3 (pYGSK3) at the base and tip of *Chlamydomonas* flagella and motile cilia in ependymal cells. The (phyto)ceramide distribution was consistent with that of a bifunctional ceramide analogue UV cross-linked and visualized by click-chemistry–mediated fluorescent labeling. Ceramide depletion, by myriocin or neutral sphingomyelinase deficiency (*fro/fro* mouse), led to GSK3 dephosphorylation and defective flagella and cilia. Motile cilia were rescued and pYGSK3 localization restored by incubation of *fro/fro* ependymal cells with exogenous C24:1 ceramide, which directly bound to pYGSK3. Our findings suggest that (phyto)ceramide-mediated translocation of pYGSK into flagella and cilia is an evolutionarily conserved mechanism fundamental to the regulation of ciliogenesis.**

Monitoring Editor
Howard Riezman
University of Geneva

Received: Jun 15, 2015
Revised: Aug 27, 2015
Accepted: Sep 30, 2015

INTRODUCTION

Flagella and cilia are slender organellar protrusions of the eukaryotic cell membrane with sensory and motor function. Flagella and cilia are similar, in that they share a microtubule-based cytoskeleton called the axoneme (Snell *et al.*, 2004; Sung and Leroux, 2013). Primary, nonmotile cilia have a ring of nine outer microtubule doublets and are studded with growth factor receptors to function as sensory organelles regulating cell migration and differentiation. Motile cilia and flagella contain two central microtubules and the motor protein dynein attached to the nine peripheral microtubule doublets (for comprehensive reviews on the structure of primary and motile cilia/flagella, see Silflow and Lefebvre, 2001; Snell *et al.*, 2004; Satir *et al.*, 2010). Motile cilia and flagella move extracellular fluids and particles and propel cells, such as sperm, and unicellular organisms, such as the green algae *Chlamydomonas reinhardtii* (Vincensini *et al.*, 2011). Flagella dysfunction leads to reduced or absent motility, whereas aberrant motile cilia lead to ependymal cell malfunction and hydrocephalus (Young *et al.*, 2013). It is vital for the signaling and motility functions of cilia that length, number, and intraciliary or intraflagellar transport (IFT) of cargo are dynamically regulated. The protein machinery regulating assembly, length, movement, and transport within these organelles is conserved from *Chlamydomonas* to

This article was published online ahead of print in MBoC in Press (http://www.molbiolcell.org/cgi/doi/10.1091/mbc.E15-06-0371) on October 7, 2015.

Address correspondence to: Erhard Bieberich (ebieberich@gru.edu).

Abbreviations used: aPKC, atypical protein kinase C; DHS, dihydrosphingosine; FB1, fumonisin B1; GSK, glycogen synthase kinase; HDAC, histone deacetylase; nSMase2, neutral sphingomyelinase 2; SPT, serine palmitoyl transferase.

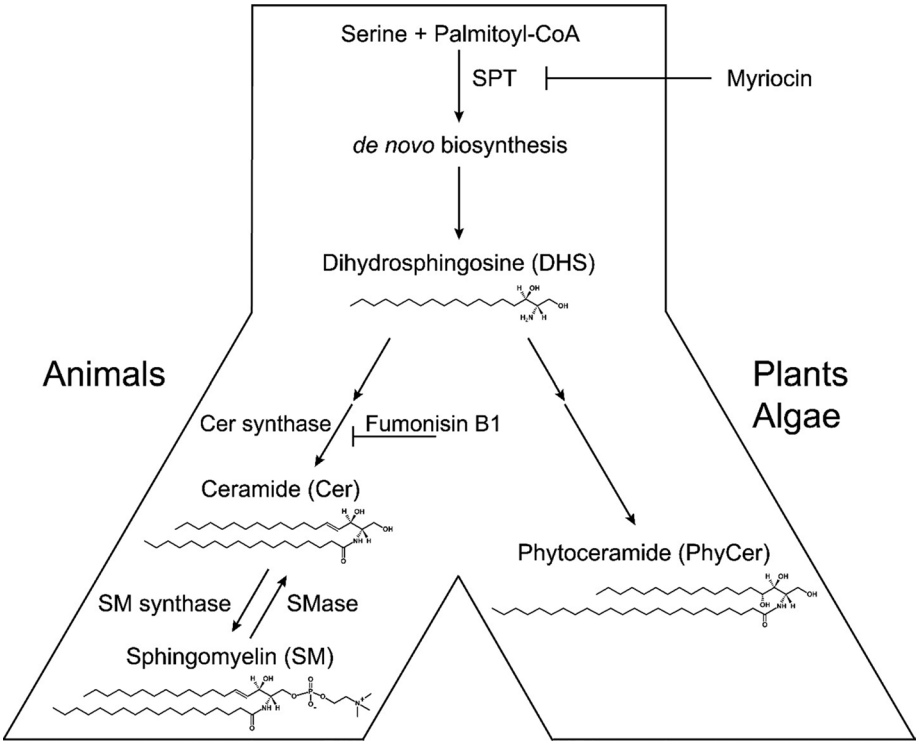

FIGURE 1: Sphingolipid metabolism in animals, plants, algae, and fungi. In animals, plants, and algae, de novo biosynthesis of ceramide and phytoceramide is initiated by conjugation of serine with palmitoyl-CoA (other activated fatty acids are possible but less frequent), a reaction catalyzed by serine palmitoyl transferase (SPT) and inhibited by myriocin. After another reaction, the intermediate dihydrosphingosine (DHS) is synthesized, which is then converted to ceramide via ceramide synthases (inhibited by fumonisin B1) in animals and phytoceramide in plants, algae, and fungi. In animals, ceramide can be converted to sphingomyelin (SM). In the cell membrane or endocytic vesicles, ceramide can be rederived from SM by hydrolysis catalyzed by sphingomyelinases (SMases). Plants, algae, and fungi do not synthesize sphingomyelin but instead inositolphosphorylsphingolipids (not shown).

mammals (Snell *et al.*, 2004; Vincensini *et al.*, 2011; Sung and Leroux, 2013). Although cilia and flagella are localized extensions of the plasma membrane, little is known about the role of lipids in this regulation of ciliogenesis and cilium function.

Sphingolipids are essential components of eukaryotic membranes and regulate vital cell signaling pathways (Bartke and Hannun, 2009; Milhas *et al.*, 2010; Bieberich, 2012; Markham *et al.*, 2013). The common long-chain base precursor for de novo biosynthesis of animal, plant, fungus, and algae sphingolipids is dihydrosphingosine (DHS; Figure 1). DHS is converted to ceramide (in animals) and phytoceramide (in plants, algae, and yeast). In animals, ceramide and its metabolite, sphingomyelin, are unique, in that their levels can be rapidly regulated by enzymatic conversion, the so-called sphingomyelin cycle (Figure 1; Hannun, 1996). Ceramide is converted to sphingomyelin by sphingomyelin synthases, whereas sphingomyelin is hydrolyzed to ceramide by acid or neutral sphingomyelinase (aSMase or nSMase respectively; Nikolova-Karakashian *et al.*, 2008; Milhas *et al.*, 2010; Shamseddine *et al.*, 2015). We previously reported that aSMase- and nSMase-mediated generation of ceramide is critical for ciliogenesis in Madin–Darby canine kidney (MDCK) cells and neural progenitors, respectively (Wang *et al.*, 2009a; He *et al.*, 2012, 2014). In contrast to mammalian cells, *Chlamydomonas* and plants do not synthesize sphingomyelin, which therefore is excluded as a source for ceramide. However, in all eukaryotic cells, ceramides can be generated by de novo biosynthesis (Figure 1; Sperling and Heinz, 2003; Gault *et al.*, 2010; Pata *et al.*, 2010; Hannun and Obeid, 2011; Markham *et al.*, 2013). The first enzyme in this pathway, serine palmitoyltransferase (SPT), can be selectively inhibited by the fungal toxin myriocin, allowing for loss-of-function experiments to examine the significance of ceramide for ciliogenesis in animal cells and algae (Miyake *et al.*, 1995; Hanada *et al.*, 2000; Wadsworth *et al.*, 2013). The long-chain base in algae and plant sphingolipids is more complex than that in animals. Hydroxylation of DHS at C4 results in biosynthesis of phytosphingosine, which can be acylated to give rise to phytoceramides (Figure 1; Spassieva *et al.*, 2002; Sperling and Heinz, 2003; Pata *et al.*, 2010; Markham *et al.*, 2013). Although plant and algae sphingolipids are relatively well known, the sphingolipid pathway in *Chlamydomonas* has not been investigated.

Physical interaction of (phyto)ceramide with proteins that are critical for ciliogenesis is likely to underlie the regulation of flagella and motile cilia, respectively. Previously, we found that in MDCK cells and human embryonic stem cell–derived neuroprogenitors, atypical protein kinase Cζ (aPKCζ) directly interacts with ceramide and promotes primary cilium extension ultimately through inhibition of histone deacetylase 6 (HDAC6; Bieberich *et al.*, 2000; Wang *et al.*, 2005, 2009b; He *et al.*, 2012, 2014). HDAC6 inhibition prevents deacetylation of lysine 40 of α-tubulin, a reaction that destabilizes microtubules and promotes cilium disassembly (Pugacheva *et al.*, 2007; Loktev *et al.*, 2008). A *Chlamydomonas* tubulin deacetylase has been described, but it is not clear whether it has the same function for flagella regulation as HDAC6 for cilia in animals (Maruta *et al.*, 1986). It is likely that ceramide interacts with additional proteins to regulate HDAC6 and/or cilium length. One candidate protein conserved in *Chlamydomonas* and mammalian cilia is glycogen synthase kinase (GSK)-3β (Wilson and Lefebvre, 2004; Thoma *et al.*, 2007). GSK-3β (GSK3) is critical for ciliogenesis, regulates HDAC6, and phosphorylates kinesin light chains that control cargo binding to microtubules (Szebenyi *et al.*, 2002; Thoma *et al.*, 2007; Song *et al.*, 2014).

To identify ceramide–protein complexes in cilia, we used chemoproteomics technology for in vitro and in vivo ultraviolet (UV) cross-linking of a bifunctional ceramide analogue (pacFACer) to interacting proteins and functionalized this covalent complex for visualization using "click chemistry" (azide-alkyne cycloaddition; see Supplemental Figure S1 for structure). In addition, we developed a novel anticeramide antibody that recognizes ceramide and phytoceramide. Using pacFACer cross-linking and anticeramide antibody, we demonstrate that *Chlamydomonas* flagella and ependymal cell cilia show a similar distribution of ceramides that bind to GSK3, which is critical for the regulation of ciliogenesis by an evolutionarily conserved mechanism of ceramide-mediated translocation of GSK3 into flagella and cilia.

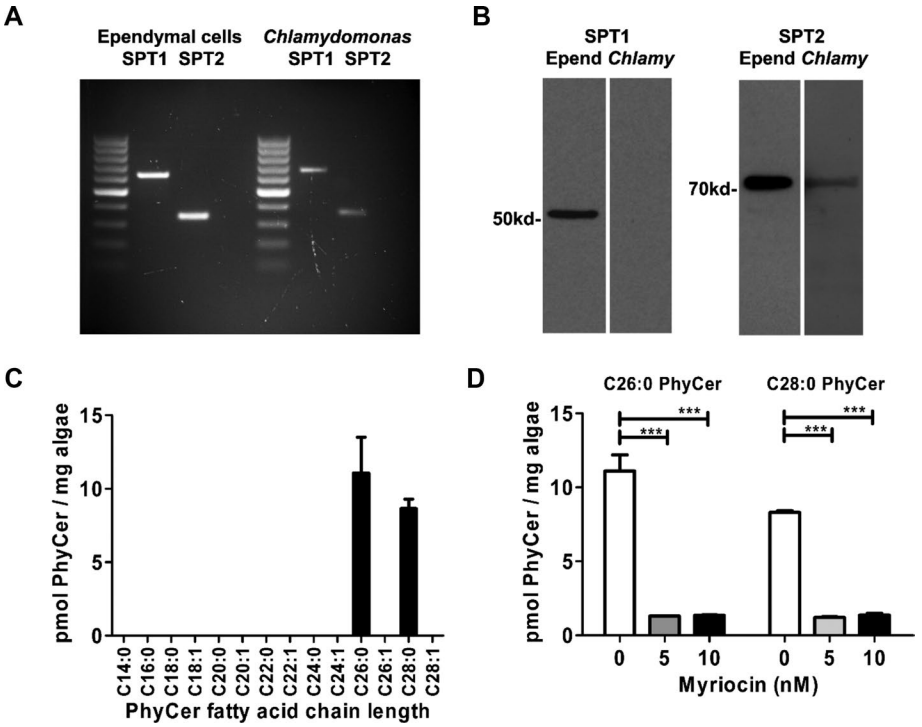

FIGURE 2: *Chlamydomonas* synthesizes phytoceramide, which can be blocked by myriocin. (A) RT-PCR using SPT1 and SPT2 primers based on the mouse genome and *Chlamydomonas* EST clones. (B) Immunoblots for SPT1 and SPT2 in mouse ependymal cells and *Chlamydomonas*. (C, D) Sphingolipidomics LC-MS/MS analysis of phytoceramides (pmol/mg *Chlamydomonas* cells) in control and myriocin-treated (5 or 10 nM) cells (15 h). Data presented show mean ± SEM, $n = 3$, $^{***}p < 0.001$ (one-way ANOVA with Bonferroni post hoc test).

RESULTS

Chlamydomonas expresses serine palmitoyltransferase and generates plant sphingolipids

There is no prior information on the presence of sphingolipids or enzymes required for sphingolipid biosynthesis in *Chlamydomonas*. Using reverse transcriptase (RT)-PCR and oligonucleotide primers based on sequence similarities between mouse serine palmitoyltransferase (SPT), the first enzyme in the sphingolipid biosynthetic pathway, and *Chlamydomonas* expressed sequence–tagged (EST) clones, we found that *Chlamydomonas* expresses mRNAs for the subunits SPT1 and SPT2 (Figure 2A). mRNAs for these SPT subunits are similar to those expressed in mouse ependymal cells enriched from primary cultured glial cells (Weibel *et al.*, 1986). In addition to SPT, we also detected mRNAs for lag1 and lag2, two ceramide synthases expressed in plants, suggesting that *Chlamydomonas* expresses several enzymes in the phytoceramide biosynthesis pathway (Supplemental Figure S1B). Expression of SPT was confirmed by immunoblot. Using an antibody raised against mammalian SPTs, we were able to detect SPT2 at the predicted molecular weight (72 kDa) but not SPT1 in *Chlamydomonas* (Figure 2B). The expression of SPTs and ceramide synthases in *Chlamydomonas* suggested that sphingolipids are synthesized. Using liquid chromatography–tandem mass spectrometry (LC-MS/MS), we found that *Chlamydomonas* generates very long chain C26:0 (11 ± 3 pmol/mg cells) and C28:0 (8 ± 2 pmol/mg cells) phytoceramides, which are common plant sphingolipids (Figure 2C). In comparison, glial cells contain relatively small proportions of phytoceramide (<10% of total ceramides; Dasgupta *et al.*, 2013) but larger amounts of ceramide (800 ± 150 pmol/mg cells), with C18:0 ceramide (35%) and C24:1 ceramide (25%) being the most abundant (Wang *et al.*, 2012). On the basis of the observation that SPT2 is expressed in *Chlamydomonas* as well as in mammalian cells, we tested the effect of myriocin, a fungal toxin and highly selective inhibitor of SPT by covalent binding to SPT2 (Wadsworth *et al.*, 2013), on (phyto)ceramide biosynthesis. Figure 2D shows that myriocin is an extremely potent inhibitor of phytoceramide biosynthesis (>90% at 5 nM) in *Chlamydomonas*, suggesting that myriocin can be effectively used to test the function of phytoceramide in *Chlamydomonas*.

Phytoceramide and ceramide are critical for motility and ciliary length regulation

On the basis of our previous studies showing that ceramide is critical for primary ciliogenesis (Wang *et al.*, 2009a; He *et al.*, 2012, 2014), we tested whether a similar function exists for the regulation of flagella in *Chlamydomonas* and motile cilia in ependymal cells. To determine the effect of inhibition of de novo sphingolipid biosynthesis by myriocin on flagella, we first performed a phototaxis motility assay (Lechtreck *et al.*, 2009). After incubation of *Chlamydomonas* in a six-well dish with 0–50 nM myriocin, half of each well was shielded from light. At 7 h, most of the algae were still motile and swimming toward light. By 15 h, only the algae not exposed to myriocin were fully motile (Figure 3A). This was confirmed both by cell counting with a hemocytometer and by measuring optical absorbance of chlorophyll at 450 nm. At a concentration of myriocin as low as 5 nM, approximately half of the cells were immotile (Figure 3B). At 10 nM myriocin, phase contrast microscopy showed that >70% of cells had extremely shortened (length <2 μm) flagella (Figure 3C) and often formed multicellular clusters (Supplemental Figure S2A). Only a small population of cells (<20%) did not show significant flagella shortening. The inhibitory effect of myriocin on cilium length and motility was reversible, since myriocin-treated cells regained motility within 48 h when resuspended in myriocin-free medium (Supplemental Figure S2B). This result was consistent with a trypan blue exclusion assay showing that myriocin-treated cells did not undergo cell death (Supplemental Figure S2C), further suggesting that the effect of myriocin on motility was specific for ciliogenesis and not due to general toxicity. To test whether the effect of myriocin was caused by reduced synthesis of sphingolipids, we performed motility rescue experiments by supplementing the medium with various sphingolipid precursors 2 h before myriocin exposure. Among the sphingolipids tested, DHS, a metabolic precursor for (phyto)ceramide biosynthesis (Figure 1), and phytoceramide itself were the most effective (60 ± 10 and 42 ± 12%, respectively) in rescuing flagella length and motility (Figure 3, D and E). Sphingosine and various ceramides were not effective for restoration of cilia (unpublished data). Fumonisin B1, a ceramide synthase inhibitor, failed to reduce motility in *Chlamydomonas*. This inhibitor has a higher dissociation constant than myriocin (100 vs. 0.28 nM) and in the case of lower uptake, the intracellular concentration of fumonisin B1 may not allow for effective inhibition of phytoceramide biosynthesis (Wang *et al.*, 1991; Miyake *et al.*, 1995). In ependymal cells, both myriocin

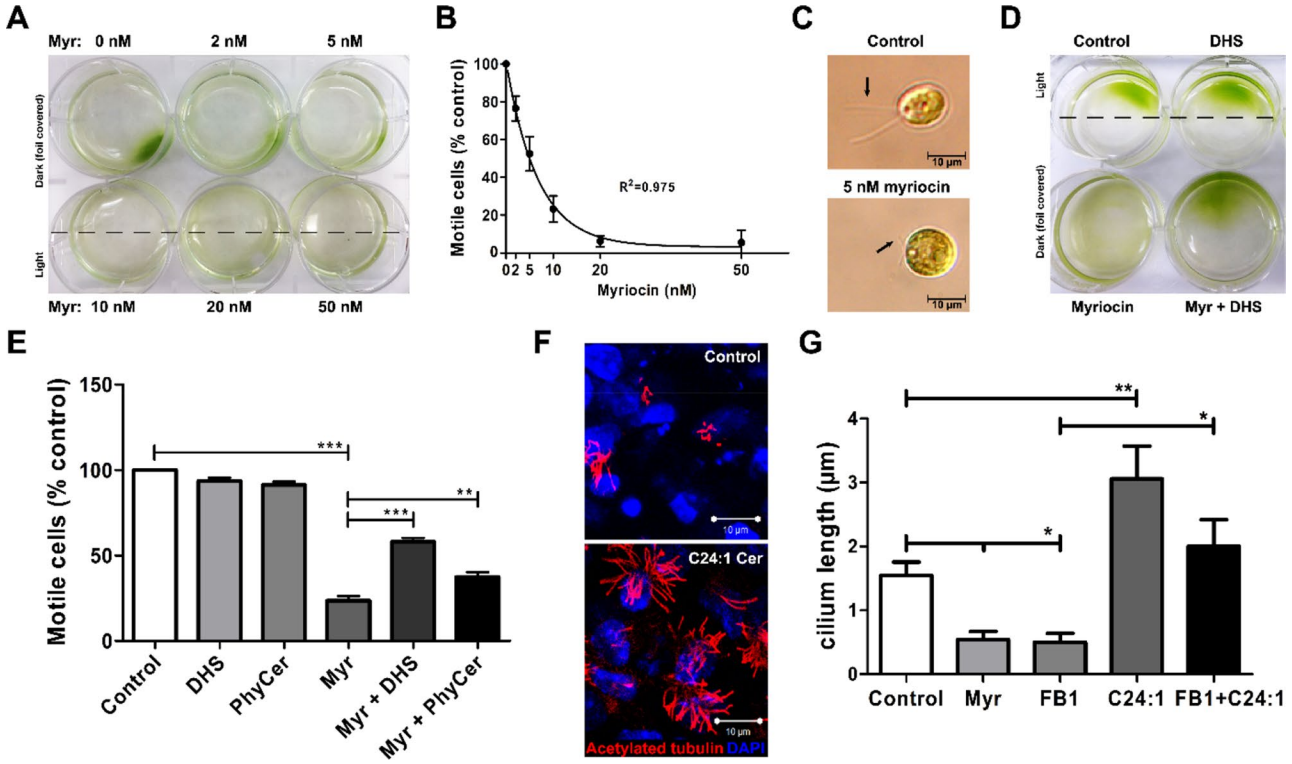

FIGURE 3: Ceramide depletion shortens cilia and leads to *Chlamydomonas* immotility, whereas exogenous DHS and C24:1 ceramide rescue *Chlamydomonas* flagella and ependymal cell cilia. All graphical data presented show mean ± SEM. (A, B) Phototaxis motility assay (15 h; $n = 5$; nonlinear regression) with *Chlamydomonas* shows prolonged incubation with myriocin (myr), which leads to (A) time- and (B) dose-dependent immotility. (C) Phase contrast of *Chlamydomonas* showing flagella shortening in myriocin-treated cells. Scale bar, 10 µm. (D) Addition of DHS (1 µM) prevents immotility in myriocin-treated cells. (E) Motility assays using DHS and phytoceramide (Phyc) to rescue flagella in myriocin-treated *Chlamydomonas* ($n = 10$, $^{**}p < 0.01$, $^{***}p < 0.001$, one-way ANOVA with Bonferroni post hoc test). (F) Immunocytochemistry using control and C24:1 ceramide (1 µM)–treated ependymal cells (red, acetylated tubulin; blue, DAPI). Scale bar, 10 µm. (G) Quantitation of motile cilium length in ependymal cells treated for 48 h with ceramide biosynthesis inhibitors (5 µM myriocin, 10 µM FB1) with or without exogenous C24:1 ceramide (1 µM; $n = 5$, $^{*}p < 0.05$, $^{**}p < 0.01$, one-way ANOVA with Bonferroni post hoc test).

and fumonisin B1 (FB1; Figure 1) reduced the length of motile cilia (Figure 3G). Addition of C24:1 ceramide to the culture medium rescued cilia in cells treated with FB1 and induced elongation of cilia in cells not treated with ceramide biosynthesis inhibitors (Figure 3, F and G). In addition to FB1-treated wild-type ependymal cells, we used cells from the *fragilitis ossium* (*fro/fro*) mouse, a mouse model for genetic deficiency of nSMase2 (Guenet *et al.*, 1981; Poirier *et al.*, 2012). In these cells, lack of nSMase2-catalyzed ceramide generation led to shortened cilia, which was rescued by exogenous C24:1ceramide (Supplemental Figure S3). Other ceramides, such as C18:0 ceramide, were not effective in rescuing cilia in ependymal cells (unpublished data). These results suggest that phytoceramides in *Chlamydomonas* and C24:1 ceramide in ependymal cells are critical for cilium length regulation, which is likely to rely on a conserved downstream mechanism.

Phytoceramide and ceramide are enriched in compartments that regulate ciliogenesis

Any effect of (phyto)ceramide on cilium regulation is likely to require the physical interaction of (phyto)ceramide with proteins in compartments that are known to regulate cilia, in particular vesicles and membranous compartments at the cilium base and the ciliary membrane. We previously generated a ceramide-specific antibody that detected an apical ceramide–enriched compartment (ACEC) at the base of primary cilia (Wang *et al.*, 2009a; Bieberich, 2011; He *et al.*, 2012, 2014). To test (phyto)ceramide distribution in *Chlamydomonas* and ependymal cells, we have generated a new antibody that reacts with both ceramide and phytoceramide as shown by lipid enzyme-linked immunosorbent assays (ELISAs; Figure 4A; data shown are background subtracted; He *et al.*, 2014; Dinkins *et al.*, 2015). This antibody does not react with fatty acid (nervonic acid was tested), but it recognizes sphingosine and phytosphingosine, which are only minor cellular sphingolipids (≤10% of (phyto)ceramide) under physiological conditions. Immunocytochemistry using this antibody showed punctate labeling for (phyto)ceramide at tips of flagella and motile cilia (Figure 4B). In addition, (phyto)ceramide was enriched in vesicles or a compartment at the bases of flagella and motile cilia (Figure 4B).

We next tested whether this compartment supplies (phyto)ceramide for the ciliary membrane. We used *Chlamydomonas* because it can be subjected to several cycles of deflagellation and reflagellation where functionality is noted by return of motility (Wilson and Lefebvre, 2004). *Chlamydomonas* was four-times deflagellated at pH 4.5, followed by rapid neutralization and reflagellation in the absence or presence of myriocin. With each de/reflagellation cycle, fewer cells retained motility. After four cycles, myriocin-treated cells completely

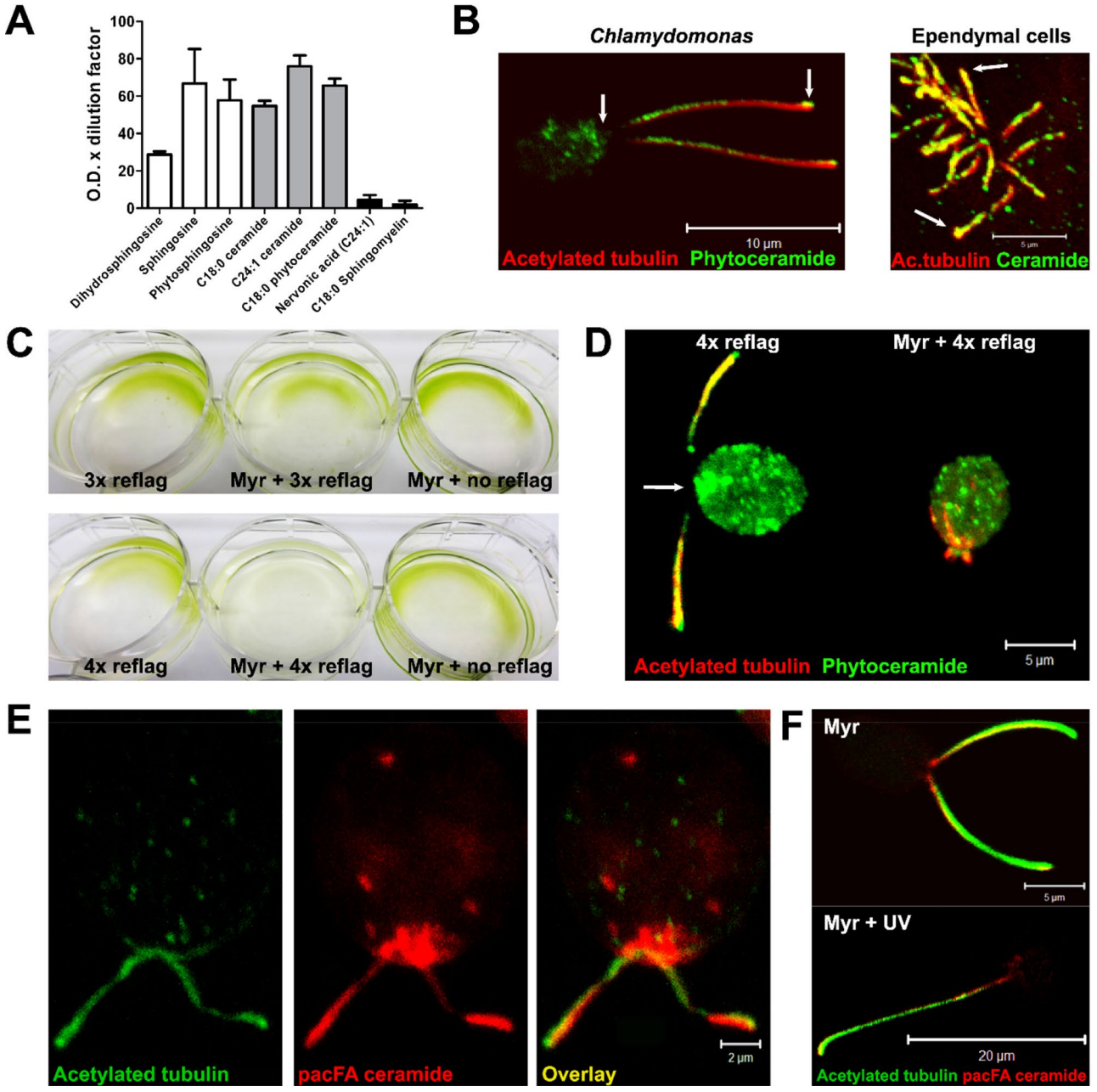

FIGURE 4: Phytoceramide and ceramide are distributed to flagella and motile cilia, respectively. (A) Lipid ELISA testing the specificity of anti-(phyto)ceramide rabbit IgG for various sphingolipids; mean ± SEM, $n = 5$. (B) Immunocytochemistry using anti-(phyto)ceramide rabbit IgG (green) and anti–acetylated tubulin mouse IgG (red) with *Chlamydomonas* and ependymal cells. In *Chlamydomonas*, arrows point at the base and tip of cilia. (C) *Chlamydomonas* was repeatedly (three or four times) de/reflagellated in the presence or absence of 10 nM myriocin. Incubation with myriocin without de/reflagellation for the duration of the experiment (5 h) was used as control. (D) Immunocytochemistry of de/reflaggelated *Chlamydomonas* in the presence or absence of myriocin using anti-(phyto)ceramide rabbit IgG (green) and anti–acetylated tubulin mouse IgG (red). (E) pacFACer (red) cross-linked in flagella tips and bases (arrowheads) colabeled with anti–acetylated tubulin (green). Visualization was performed by labeling the cross-linked ceramide analogue with Alexa 594 using click chemistry. (F) UV cross-linking of pacFACer (red) followed by de/reflagellation led to formation of single, long flagella, which was absent when cells were incubated with pacFACer without UV cross-linking (anti–acetylated tubulin, green). Scale bars, 10 µm (B, left), 5 µm (B, right), 5 µm (D), 2 µm (E), 5 µm (F, top), 20 µm (F, bottom).

lost motility, whereas control cells were not affected (Figure 4C). In contrast to overnight incubation (Figure 3A), continuous myriocin incubation for 5 h of cells not undergoing de/reflagellation did not show loss of motility. Immunocytochemistry using the anti-(phyto)ceramide antibody showed that loss of motility in myriocin-treated cells undergoing repeated de/reflagellation was concurrent with the inability to regrow flagella and disappearance of the (phytoceramide-enriched compartment at the flagella base (Figure 4D). This result suggests that the phytoceramide-enriched compartment in the cell body is dependent on de novo phytoceramide biosynthesis and

supplies phytoceramide for the flagellar membrane. In the presence of myriocin, phytoceramide transported into the flagellar membrane and lost by repeated deflagellation can no longer be replenished from the cell body, and flagella are no longer formed.

To test whether phytoceramide is cotransported with proteins from the base into flagella, we used a bifunctional ceramide analogue, pacFA Ceramide (pacFACer; Supplemental Figure S1A) to covalently label protein interaction partners of phytoceramide in the compartment at the flagella base and the flagellar membrane. After UV cross-linking, the pacFACer–protein complex was visualized by covalent linking to Alexa Fluor 594 azide using click chemistry. Alexa Fluor 594–labeled pacFACer was enriched in the base and tip of flagella (Figure 4E), consistent with the results obtained with anti-(phyto)ceramide antibody (Figure 4B). Next we incubated *Chlamydomonas* with pacFACer, followed by UV cross-linking and one cycle of de/reflagellation in the presence of myriocin before labeling of the pacFACer–protein complex with Alexa Fluor 594 azide. A proportion of the cells (15 ± 5%) formed single, very long (20 ± 3 μm) flagella approximately double the length of normal flagella, which was not observed in the absence of UV cross-linking (Figure 4F). In these cells, the ceramide-enriched compartment at the flagella base was absent, consistent with the results obtained from repeated de/reflagellation (Figure 4D). The formation of a single, elongated flagellum labeled with pacFACer suggests that the pacFACer–protein complex is cross-linked at the flagella base and is then transported into the newly formed flagellum. Failure to dissociate after initial binding and transport due to covalent cross-linking leads to irreversible membrane association and excess cilium extension, similar to the phenotype of *Chlamydomonas* mutants with defective protein kinases involved in cilium length regulation (Berman *et al.*, 2003; Wilson and Lefebvre, 2004; Hilton *et al.*, 2013). These results suggest that (phyto)ceramide at the cilium base transiently interacts with proteins, in particular protein kinases that are critical for cilium length regulation.

Motile ciliogenesis in *Chlamydomonas* and ependymal cells relies on active GSK-3β

One of the protein kinases that are highly conserved from *Chlamydomonas* to mammals and critical for ciliogenesis is GSK-3β. In *Chlamydomonas,* whose genome encodes for a single GSK3 isoform, activated pYGSK3 has been shown to be enriched in flagella and to regulate flagellar length (Wilson and Lefebvre, 2004). We performed immunoblotting of proteins from myriocin-treated *Chlamydomonas* and found a reduction of pYGSK3 levels, which was prevented by exogenous DHS, the phytoceramide precursor (Figure 5A). Consistently, acetylated tubulin was also reduced by myriocin and rescued by DHS, supporting the hypothesis that pYGSK3 levels are correlated with tubulin acetylation in flagella. In addition to pYGSK3, total GSK3 levels were reduced by myriocin and rescued by DHS, suggesting that ceramide depletion leads to decreased expression or increased degradation of *Chlamydomonas* GSK3.

To show the direct effect of GSK3 activity on flagella and cilia, we incubated *Chlamydomonas* and ependymal cells with (2′Z,3′E)-6-bromoindirubin-3′-oxime (BIO), a highly selective GSK3 inhibitor (Sato *et al.*, 2004), for 60 min. GSK3 inhibition led to immotility and flagellar length reduction (Figure 5B) similar to that observed with myriocin (Figure 3C), which is consistent with the hypothesis that phytoceramide and ceramide are critical for activation of GSK3 to regulate cilium length. Lithium chloride, a noncompetitive GSK3 inhibitor, also led to immotility, although flagella were first elongated (after 2-h incubation; Figure 5B) and then lost (after 24 h; unpublished data) consistent with previous studies (Wilson and Lefebvre, 2004).

The enrichment of pYGSK3 in flagella indicates that it may be colocalized with phytoceramide and ceramide in *Chlamydomonas* and ependymal cells, respectively. We found that pYGSK3 was colocalized with phytoceramide in the flagellar membrane, particularly in the flagella tips (Figure 5C). In ependymal cells, cilia were colabeled for pYGSK3 and ceramide (Figure 5D). Of interest, we found that whereas pYGSK3 colocalized with acetylated tubulin in cilia (Figure 5E, left), inactive GSK3 phosphorylated at ser9 (pSGSK) was not found in cilia (Figure 5E, right). This result suggested that pYGSK3 may bind directly to ceramide in the ciliary membrane. A lipid ELISA-based binding assay using recombinant human GSK-3β expressed in Sf9 cells confirmed that GSK3 binds to different ceramide species (Figure 5F). Affinity of human GSK3 was highest to C24:1 ceramide, which was able to rescue cilia in ceramide-depleted ependymal cells (Figure 3, F and G). Immunoblots showed that human GSK3 was phosphorylated at Tyr-216, consistent with the hypothesis that pYGSK3 binds directly to ceramide (Figure 5G).

Immunoblots of ependymal cells from wild-type and *fro/fro* mice showed reduced pYGSK3 and increased pSGSK3 in *fro/fro* cells, suggesting that reduced cellular ceramide leads to less activation of GSK3 (Figure 6A), concurrent with reduced cilium length and diminished labeling of pYGSK3 in motile cilia (Figure 6B and Supplemental Figure S3). Immunohistochemistry on cryosections of *fro/fro* brains showed that the length of motile cilia in the ependyma was also reduced by >50% (Figure 6, C and D). Motile cilia in the ependyma showed colocalization of ceramide with pYGSK3, predominantly in punctate structures along the membrane and cilium tip (Figure 6, E and F), which was consistent with the results obtained with primary cultured ependymal cells (Figure 6, B and C). Taken together, these results suggest that phytoceramide and ceramide may induce activation and translocation of pYGSK3 into flagella and cilia, which is instrumental for the regulation of their length.

Ceramide interaction with aPKCζ regulates ciliogenesis in ependymal cells

Our previous studies showed that aPKCζ, another protein kinase that directly binds to ceramide, regulates primary ciliogenesis in mammalian cells (Lozano *et al.*, 1994; Muller *et al.*, 1995; Wang *et al.*, 1999; Bieberich *et al.*, 2000; Bourbon *et al.*, 2000; Fan *et al.*, 2004; Ossipova *et al.*, 2007; Pruliere *et al.*, 2011; He *et al.*, 2012, 2014). GSK-3β can be inactivated by aPKCζ-mediated phosphorylation of Ser-9 (pSGSK3), suggesting that mammalian ciliogenesis can be regulated by binding of ceramide to both GSK-3β and aPKCζ (Etienne-Manneville and Hall, 2003; Kim *et al.*, 2007; Krishnamurthy *et al.*, 2007b). Genome analysis shows that plants and *Chlamydomonas* do not express a homologue of aPKCζ, and GSK3 does not contain an equivalent to the Ser-9 phosphorylation site found in mammalian GSK-3β (Kruse *et al.*, 1996; Wilson and Lefebvre, 2004). Therefore we limited the analysis of motile cilia regulation by ceramide and aPKCζ to ependymal cells. An orthogonal view of a confocal *z*-scan shows that UV cross-linked pacFACer colocalizes with aPKCζ in the ceramide-enriched compartment at the cilium base (Figure 7A). The physical interaction of pacFACer with aPKCζ was demonstrated by a lipid ELISA-based assay using a surface coat of pacFACer for binding to recombinant aPKCζ. Binding was enhanced by UV cross-linking, suggesting that aPKCζ could be covalently linked to pacFACer and is indicative of high affinity for ceramide. The reaction did not occur in the absence of pacFACer (pCer), aPKCζ, or aPKCζ-specific antibody (Figure 7B). The ceramide binding affinity of aPKCζ was tested using lipid ELISA with

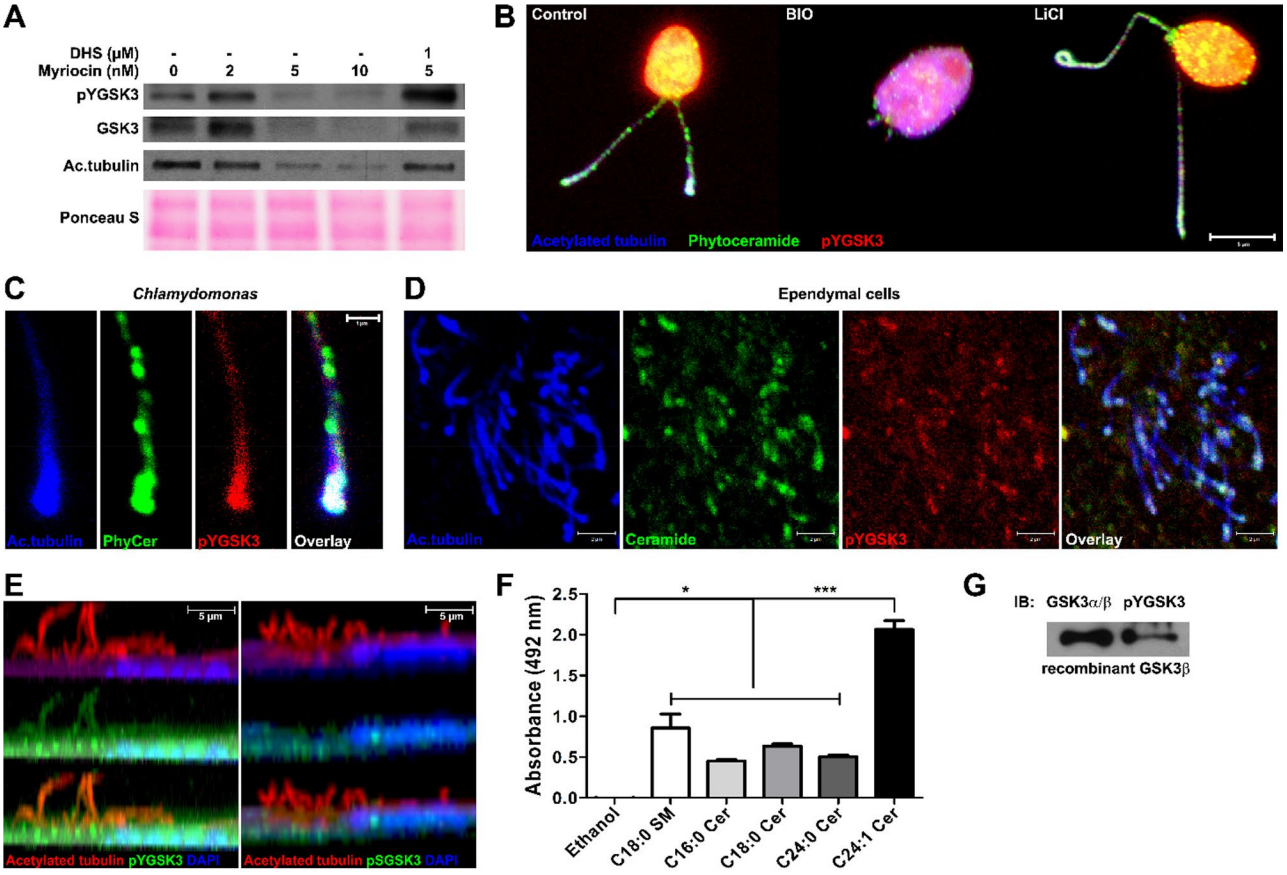

FIGURE 5: (Phyto)ceramide binds to pYGSK3 and sustains its phosphorylation level and localization in flagella and cilia. (A) Immunoblot of pYGSK, total GSK3, and acetylated tubulin from *Chlamydomonas* treated for 24 h with myriocin (5 or 10 nM) ± 1 μM DHS. Bottom, Ponceau S staining for loading control. (B) Immunocytochemistry using antibodies against (phyto)ceramide rabbit (green), pYGSK (red), and acetylated tubulin (blue) with *Chlamydomonas* incubated for 60 min with GSK3β inhibitor BIO (2 μM) or lithium chloride (25 mM). (C) Higher magnification of flagella in left side of B. (D) Same as in B and C with ependymal cells (*Z*-scan projection). (E) *Z*-scan orthogonal view of ependymal cells labeled with DAPI (blue) and antibodies against acetylated tubulin (green), pYGSK (green; left), and pSGSK (green; right). (F) C18 sphingomyelin and indicated ceramides were coated on ELISA plates and bound to recombinant GSK-3β; binding was quantified by development with anti-GSK-3α/β IgG and anti-mouse IgG-HRP. Mean ± SEM, $n = 3$, *$p < 0.05$, ***$p < 0.001$. (G) Immunoblot showing reactivity of recombinant human GSK-3β with anti-pYGSK3 IgG. Scale bars, 5 μm (B), 1 μm (C), 2 μm (D), 5 μm (E).

surface coats of ceramides differing in the chain length and degree of saturation of the fatty acid moiety. Affinity of aPKCζ was higher for ceramides with very long chain and unsaturated fatty acids, with highest affinity for C24:1 ceramide (Figure 7C), similar to the affinity found with GSK-3β (Figure 5F). This result is consistent with rescue of cilia length in myriocin-treated ependymal cells and elongation of cilia in untreated cells by C24:1 ceramide.

We tested whether aPKCζ activation or inhibition is critical for ceramide-regulated motile ciliogenesis. Incubation of ependymal cells with FB1, a ceramide synthase inhibitor, led to reduction of motile cilium length (Figure 7D). The cell-permeable myristoylated aPKCζ pseudosubstrate inhibitor (PZI) prevented reduction of motile cilium length by FB1, suggesting that ceramide-mediated inhibition of aPKCζ is critical for motile ciliogenesis (Figure 7D). Consistent with this hypothesis, addition of PZI to cells not treated with FB1 resulted in increase of cilium length by 50–60% (Figure 7D). Taken together, these results suggest that in ependymal cells, ceramide binds and inhibits aPKCζ, which leads to increase of cilium length. However, because colocalization of aPKCζ with ceramide was detected only at the cilium base but not in the ciliary membrane (Figure 7A), we concluded that binding of aPKCζ to ceramide at the cilium base affects a secondary target that regulates cilium length by its translocation into cilia. Consistent with the observation that GSK3 is critical for flagella formation and a target for mammalian aPKCζ, we found that inhibition of GSK3 with BIO obliterated motile cilia in ependymal cells (Figure 7D). Therefore we hypothesize that GSK3 is this secondary target by being phosphorylated at Ser-9 and inactivated by aPKCζ, unless aPKCζ is bound to ceramide at the cilium base and sequestered from GSK3 that is translocated to the ciliary membrane.

DISCUSSION

Length regulation of primary and motile cilia and flagella is essential for their biological function. More than 20 proteins are known to regulate cilium length, among which are many protein kinases (e.g., Aurora A kinase [AurA], MAPK/MAK/MRK overlapping kinase or MOK/RAGE1), IFT proteins, and enzymes involved in tubulin modification (e.g., HDAC6; Pan *et al.*, 2004; Pugacheva *et al.*, 2007;

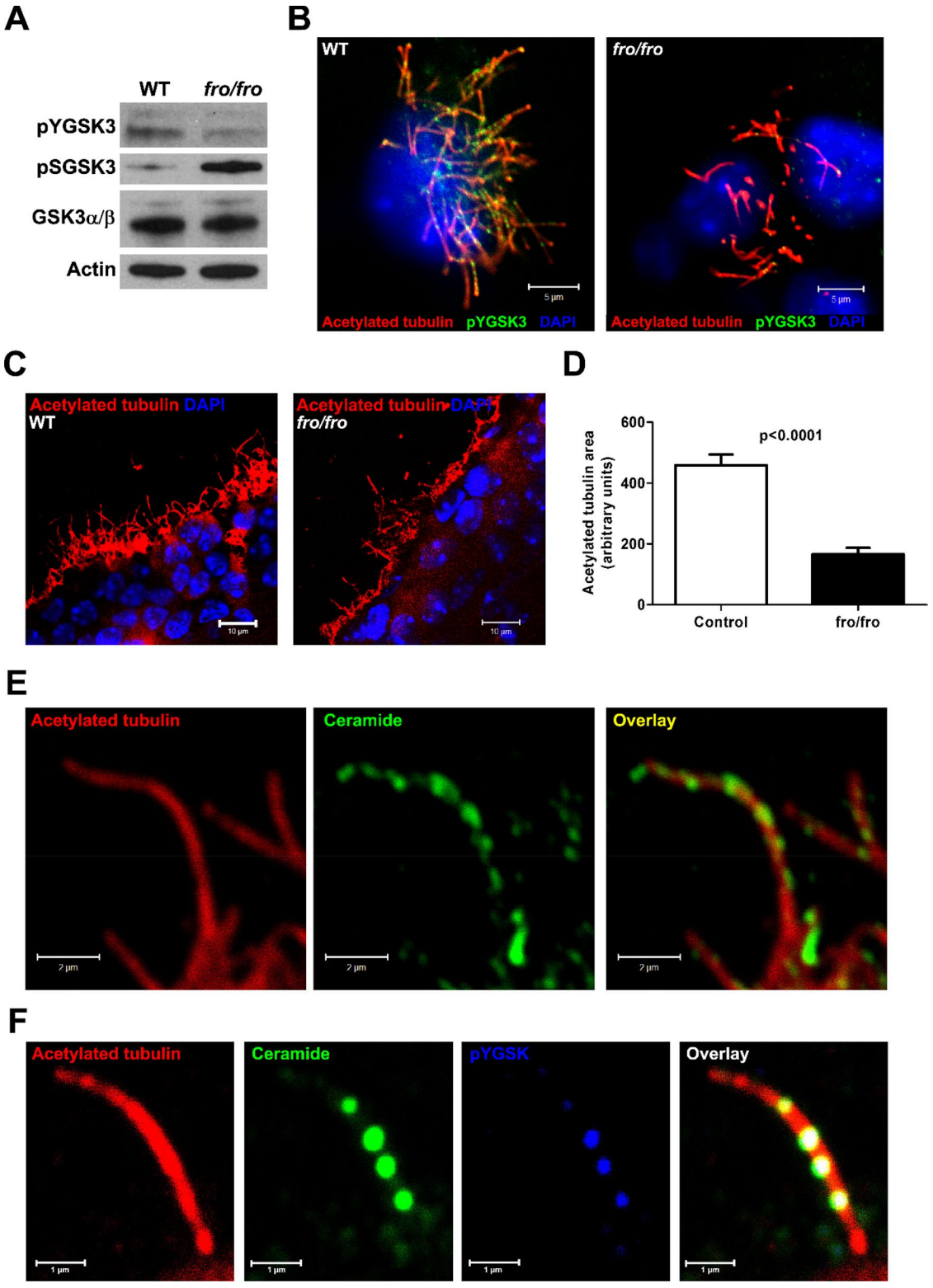

FIGURE 6: nSMase2 deficiency leads to shortening of motile cilia in vivo. (A) Immunoblot for pYGSK3, pSGSK3, and total GSK-3α/β using lysates from wild-type and *fro/fro* ependymal cells. (B) Immunocytochemistry shows that pYGSK (green) is transported to cilia tips (arrows) in wild-type but not in *fro/fro* ependymal cells. (C) Immunocytochemistry for acetylated tubulin (red) comparing cryosections of wild-type and *fro/fro* brain (3-mo-old mice) shows that cilia are shorter in nSMase2-deficient ependymal cells. (D) Quantitation of A. Mean ± SEM, $n = 3$, 10 sections/mouse. Student's *t* test, $p < 0.0001$. (E) Immunocytochemistry for ceramide (green) shows punctate labeling along the ciliary membrane and tip. (F) Ceramide (green) is colocalized with pYGSK (blue). White punctae indicate colocalization of ceramide, pYGSK, and acetylated tubulin (red). Scale bars, 5 μm (B), 10 μm (C), 1 μm (E, F).

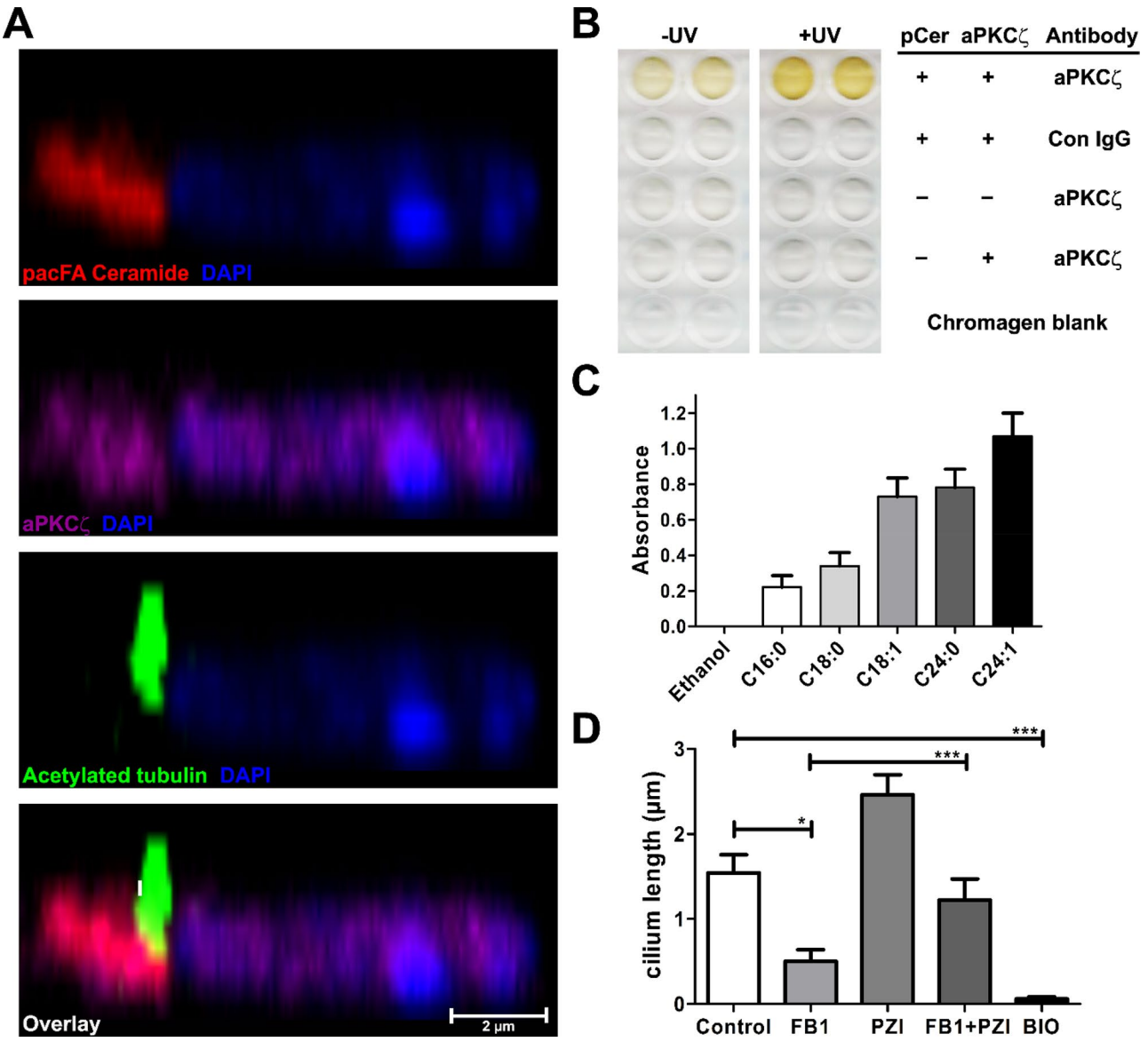

FIGURE 7: Ceramide binds to aPKCζ, whose inhibition leads to cilium length extension. (A) pacFACer was UV cross-linked to protein in primary cultured ependymal cells, linked to Alexa Fluor 594 azide (red), and labeled with anti-aPKCζ (magenta) and anti–acetylated tubulin (green) antibodies. Scale bar, 2 μm. (B) pacFACer was coated on ELISA plates and recombinant aPKCζ cross-linked by UV (365 nm) radiation. Presence/absence of pacFACer (pCer) and recombinant aPKCζ along with primary antibody used. (C) Indicated ceramides were coated on ELISA plates and bound to recombinant aPKCζ, and binding was quantified by development with anti-aPKCζ IgG and anti-rabbit IgG-HRP. Mean ± SEM, $n = 3$. (D) Incubation of ependymal cells (24 h) with FB1 (10 μM) reduces cilium length, whereas addition of aPKCζ inhibitor PZI (10 μM) leads to extension of untreated or (partial) restoration of FB1-treated cilia. The GSK-3β inhibitor BIO (2 μM) obliterates cilia. Data presented show mean ± SEM, $n = 5$, $^{*}p < 0.05$, $^{***}p < 0.001$ (one-way ANOVA with Bonferroni post hoc test).

Cao *et al.*, 2013; Broekhuis *et al.*, 2014). Little is known about the dynamic role of lipids in ciliogenesis. Because the cell membrane cannot be stretched, any cilium length extension is inevitably accompanied by net synthesis and transport of membrane lipids by either vesicle traffic or lateral movement of lipids within the cell membrane toward the cilium base. While new membrane is added at the cilium base, tubulin and other proteins for cilium extension are transported along the cilium and then added at the tip. It is not clear how membrane lipid and protein transport are coregulated to ensure that elongation of the axoneme is adjusted to the adequate expansion of the ciliary membrane. Our study presents new evidence that the sphingolipid (phyto)ceramide is instrumental for length regulation of flagella and cilia, based on data from the green algae *Chlamydomonas* flagella and murine ependymal cells.

Chlamydomonas is a well-established model to study regulation of motile cilium length by testing mechanisms that affect flagella growth and regeneration. It has been shown that the flagellar membrane is enriched with phosphatidylethanolamine, which can be hydrolyzed by phospholipase D (PLD) to phosphatidic acid (PA), a lipid known to induce deflagellation (Quarmby *et al.*, 1992; Goedhart

and Gadella, 2004; Lechtreck *et al.*, 2013). However, it is not clear whether PLD-mediated generation of PA is part of a process regulating flagella length. It is also not known whether *Chlamydomonas* expresses enzymes that generate sphingolipids and whether these lipids, if present, are essential for regulation of flagella. Using RT-PCR and immunoblotting. we showed that SPT, the first enzyme in de novo sphingolipid biosynthesis, and in particular its subunit SPT2, is conserved and expressed in *Chlamydomonas*. LC-MS/MS confirmed that C26:0 and C28:0 phytoceramide are generated, suggesting that *Chlamydomonas* expresses a complete set of enzymes for de novo sphingolipid biosynthesis. Although the analysis of the complete set of enzymes in (phyto)ceramide biosynthesis is part of our future studies, we could show that *Chlamydomonas* expresses the mRNAs of two putative ceramide synthases, lag1 and lag2. Among the enzyme inhibitors tested, the SPT inhibitor myriocin blocked phytoceramide biosynthesis and led to flagella length reduction and immotility. The specificity of this effect was demonstrated by the recovery of flagella growth and motility after removal of myriocin and by rescuing flagella with exogenous DHS, a downstream product of SPT and precursor for phytoceramide. Flagella were also partially rescued by exogenous phytoceramide, suggesting that flagella length is regulated by DHS that is metabolically converted to phytoceramide. Exogenous ceramide did not rescue flagella in *Chlamydomonas*, but it prevented loss of motile cilia in ependymal cells treated with inhibitors of ceramide biosynthesis. These results demonstrate that phytoceramide and ceramide are ciliogenic sphingolipids that regulate cilium length in *Chlamydomonas* and ependymal cells, respectively.

In animals, ceramide is synthesized in the endoplasmic reticulum (ER), transported to the Golgi, where it can be converted into glycosphingolipids or sphingomyelin, which are further transported to the cell membrane. Sphingomyelin can be internalized by endocytosis and hydrolyzed to ceramide by sphingomyelinases (SMases). Our previous studies have shown that SMases in mammalian cells generate ciliogenic ceramide that is accumulated in an ACEC at the base of primary cilia (Wang *et al.*, 2009a; He *et al.*, 2012, 2014). In plants and yeast, phytoceramide is also synthesized in the ER and derivatized to complex phytosphingolipids in the Golgi. However, plants and algae do not contain sphingomyelin, but instead they generate inositolphosphorylsphingolipids (Lester and Dickson, 1993; Sperling and Heinz, 2003; Markham *et al.*, 2013). Therefore phytoceramide in *Chlamydomonas* is likely to be generated at the flagella base, either by de novo biosynthesis or degradation of complex phytosphingolipids, and then further transported into the ciliary membrane. This transport was tested using two techniques: labeling of phytoceramide and ceramide with an antibody and direct fluorescent labeling of the bifunctional ceramide analogue pacFACer after UV cross-linking to interacting protein(s). Anti-ceramide immunoglobulin G (IgG) was originally generated in our laboratory and has been extensively tested in independent laboratories using immunocytochemistry (Krishnamurthy *et al.*, 2007a; Wang *et al.*, 2009a; Muscoli *et al.*, 2010; He *et al.*, 2012, 2014). Anti-ceramide IgG was found to detect ceramide and phytoceramide in lipid ELISAs (He *et al.*, 2014; Dinkins *et al.*, 2015). Using this antibody, we showed that phytoceramide and ceramide are enriched at the base and the tip of flagella and motile cilia in *Chlamydomonas* and ependymal cells, respectively. These results suggest that (phyto)ceramide is transported from the ciliary base to the tip.

Figure 8A shows a model consistent with cotransport of (phyto) ceramide and flagella/cilia length-regulating proteins. In this "flux equilibrium model," lipid vesicles from the ceramide compartment are incorporated into the ciliary membrane at the cilium base. Lipid–cargo protein cotransport ensures the stoichiometry required for simultaneous cilium elongation and membrane expansion. (Phyto)ceramide may serve as a membrane anchor for cotransported cargo proteins, or, alternatively, it may activate a loading/unloading mechanism at the base or tip of the cilium. The cilium length is regulated by the size or ceramide content of the compartment at the base and its lipid flux to the cilium: more ceramide favors cilium assembly, and less favors disassembly, until flux rates in both directions are equal and the cilium length is maintained. Consistent with this model, repeated deflagellation and reflagellation in the presence of myriocin led to the inability to regenerate flagella, indicating that phytoceramide is continuously incorporated into the ciliary membrane and replenished by de novo biosynthesis. Appearance of fluorescently labeled pacFACer in newly formed flagella was concurrent with disappearance of labeling at the base, further supporting the hypothesis that (phyto)ceramide is transported from the base into the ciliary membrane.

Any specific regulation of cilia by (phyto)ceramide requires its interaction with proteins involved in ciliogenesis. It has been shown that several evolutionary conserved kinases with mammalian homologues, such as *Chlamydomonas* AurA-like kinase, LF4p (MOK in mammals), and GSK3 are important for flagella length regulation (Silflow and Lefebvre, 2001; Berman *et al.*, 2003; Pan *et al.*, 2004; Wilson and Lefebvre, 2004; Thoma *et al.*, 2007; Cao *et al.*, 2009, 2013; Ou *et al.*, 2009; Hilton *et al.*, 2013; Broekhuis *et al.*, 2014). GSK3 is of particular importance since its role in ciliogenesis has been confirmed in numerous studies, but it is unclear whether cilium length extension is induced by activation or inhibition of GSK3, or both. Lithium chloride, a noncompetitive inhibitor of GSK3, has been shown to induce cilium extension in *Chlamydomonas* and mammalian cells (Berman *et al.*, 2003; Nakakura *et al.*, 2014). However, LiCl is not specific and requires millimolar concentrations for effectiveness, and other studies have shown that its effect on ciliogenesis is independent of GSK3 (Ou *et al.*, 2009). Specific GSK3 inhibitors have not been tested in *Chlamydomonas,* and they have given inconsistent results when used to test their effect on mammalian ciliogenesis (Ou *et al.*, 2009; Wang *et al.*, 2009a). We administered two specific GSK3 inhibitors, BIO and indirubin-3-monoxime, to *Chlamydomonas* and found that they lead to complete shortening of flagella within 60 min, consistent with their effect on ependymal cells. Therefore we conclude that active GSK3 is critical for maintenance or extension of cilia. This conclusion is consistent with previous studies showing that active pYGSK3 is translocated into flagella and that GSK3 knockdown leads to flagella shortening (Wilson and Lefebvre, 2004). It is also consistent with studies showing that specific inhibition or knockdown of GSK3 impairs ciliogenesis in mammalian cells (Ou *et al.*, 2009). The critical role of pYGSK3 for ciliogenesis was further substantiated by our observation that pYGSK3 is colocalized with phytoceramide and ceramide in *Chlamydomonas* flagella and ependymal cell motile cilia, respectively. In ependymal cells, nSMase2 deficiency led to decreased levels of pYGSK and increased levels of pSGSK, clearly showing that nSMase2-mediated generation of ceramide is instrumental for increasing pYGSK3 and reducing pSGSK levels.

Activation of GSK3 by autophosphorylation of Tyr-216 is a cotranslational process, whereas inactivation by desphosphorylation at this residue and phosphorylation of Ser-9 are posttranslational and regulated by phosphatases and kinases, respectively (Beurel *et al.*, 2015). Because nSMase2-deficient ependymal cells show reduction of Tyr-216 and increase of Ser-9 phosphorylation, ceramide is likely to affect phosphatases and kinases that regulate GSK3 phosphorylation. We and other laboratories have found that ceramide binds

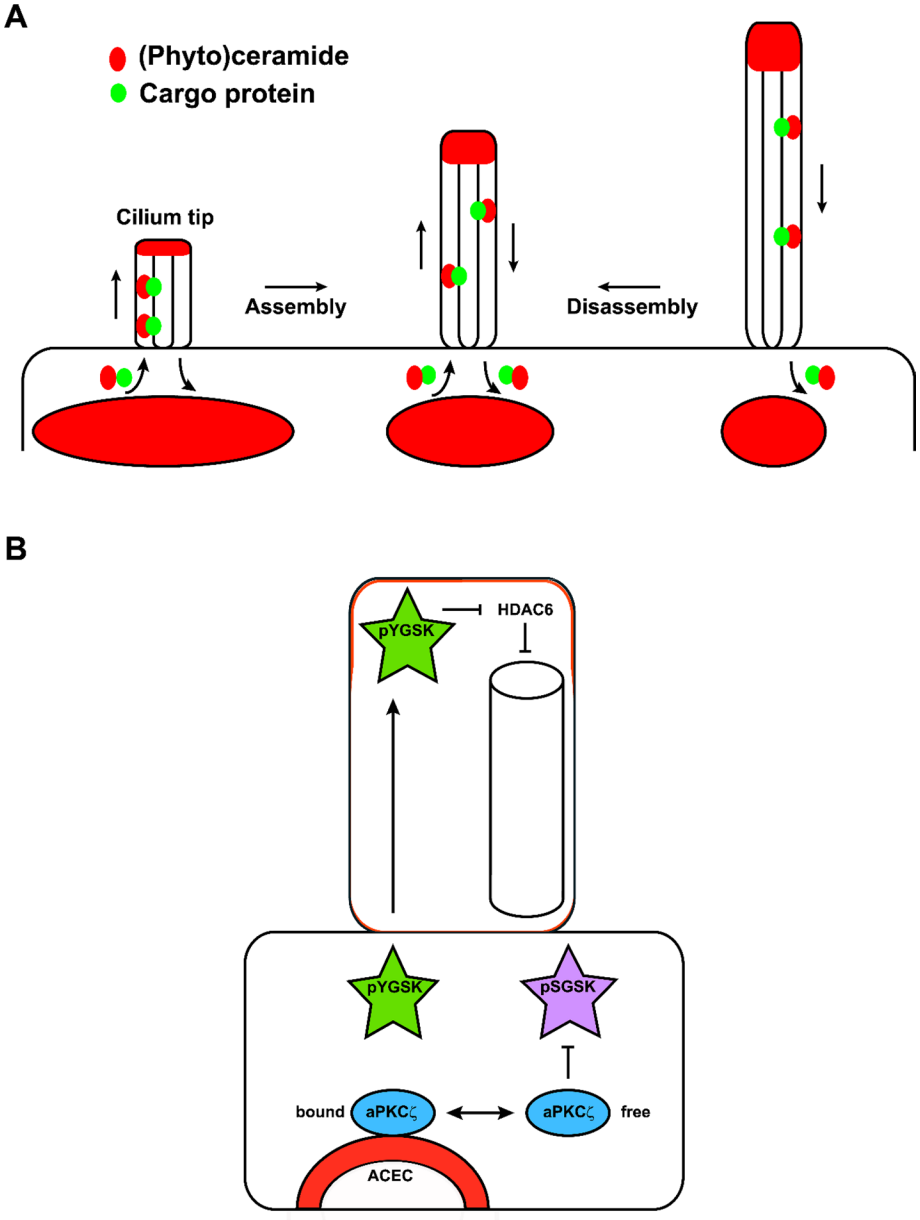

FIGURE 8: Model for flagella/cilia length regulation by (phyto)ceramide. (A) Flux equilibrium model. Lipid vesicles from the ceramide compartment (red) are incorporated into the ciliary membrane at the cilium base. Lipid–cargo protein (green) cotransport ensures the stoichiometry required for simultaneous cilium elongation and membrane expansion. (Phyto)ceramide may serve as a membrane anchor for cotransported cargo proteins, or, alternatively, it may activate a loading/unloading mechanism at the base or tip of the cilium. The cilium length is regulated by the size or ceramide content of the compartment at the base and its lipid flux to the cilium: more ceramide favors cilium assembly and less favors disassembly, until flux rates in both directions are equal and the cilium length is maintained. (B) Regulation of GSK3 by (phyto) ceramide. In *Chlamydomonas* and ependymal cells, (phyto)ceramide binds to pYGSK3 at the ceramide-enriched compartment (ACEC) and transports it to flagella/cilia. In ependymal cells, ACEC-resident ceramide (red) binding and sequestration of aPKCζ prevent inactivation of GSK-3β by aPKCζ-mediated phosphorylation of Ser-9, which complements activation and transport of pYGSK3. In the cilium tip, pYGSK3 down-regulates HDAC6 or induces cargo release from the motor protein complex, most likely regulated by its interaction with (phyto)ceramide.

and sequesters aPKCζ (Lozano *et al.*, 1994; Muller *et al.*, 1995; Wang *et al.*, 1999, 2005, 2009b; Bieberich *et al.*, 2000; Bourbon *et al.*, 2000; Fox *et al.*, 2007), which was confirmed by lipid ELISAs and UV cross-linking to pacFACer. Ceramide-induced sequestration may prevent aPKCζ-mediated phosphorylation of GSK3 at Ser-9 and lead to enrichment of pYGSK3 in the cilium tip (Figure 8B). The hypothesis that ceramide-mediated sequestration of aPKCζ is critical for cilium length extension is supported by the observation that inhibition of aPKCζ with PZI promotes ciliogenesis in ependymal cells. Ceramide depletion prevents sequestration of aPKCζ and enrichment of pYGSK3 in cilia, whereas it promotes phosphorylation of GSK3 at Ser-9 and elevation of pSGSK3 levels (Figure 6A). Neither aPKCζ nor pSGSK3 is transported into cilia, suggesting that ciliary pYGSK3 is critical for cilium length regulation.

In *Chlamydomonas*, pYGSK3 levels and transport into flagella are elevated by phytoceramide, but the interaction partner is unknown, as plants and algae do not possess aPKC homologues (Kruse *et al.*, 1996). Moreover, *Chlamydomonas* GSK3 does not have a phosphorylation site homologous to Ser-9 in mammalian GSK-3β (Wilson and Lefebvre, 2004). Therefore phytoceramide may sustain pYGSK3 levels and its enrichment into flagella by a different mechanism. Our data showing that phytoceramide is colocalized with pYGSK3 in flagella strongly suggest that phytoceramide may regulate IFT of pYGSK3 (Figure 8B). Similarly, colocalization of ceramide with pYGSK3 in motile cilia suggests that ceramide may interact directly with pYGSK3 within the ciliary membrane and promote its transport to the tip. Support for this hypothesis comes from lipid-based ELISAs showing that recombinant human GSK-3β binds to C24:1 ceramide, the ceramide species rescuing motile cilia in ceramide-depleted ependymal cells. Potential binding to pYGSK3 may be the evolutionarily older mechanism by which (phyto)ceramide regulates flagella/cilia, whereas ceramide-mediated sequestration of aPKC may have developed more recently as a complementary mechanism of GSK3 activation in animals.

It is unknown how the interaction of phytoceramide or ceramide with pYGSK3 in the cilium tip may regulate cilium length extension. It is possible that pYGSK down-regulates HDAC6, thereby preserving tubulin acetylation (Figure 8B). Support for this hypothesis comes from a previous study showing that dysfunctional GSK3 leads to up-regulation of HDAC6 and ciliary defects (Song *et al.*, 2014). It is also possible that pYGSK does not directly regulate tubulin acetylation but instead cargo release at the cilium tip. It has been shown that GSK3-mediated phosphorylation of kinesin light chain leads to release of transport vesicles in neuronal axons (Szebenyi *et al.*, 2002). It is likely that a similar mechanism may induce phosphorylation of kinesin 2 in cilia, which then allows for release of proteins that are critical for cilium assembly at the tip.

The interaction of phytoceramide and ceramide with pYGSK at the cilium tip may trigger this cargo release and promote ciliogenesis.

In summary, our study shows that (phyto)ceramide is critical for the regulation of flagella in *Chlamydomonas* and motile cilia in ependymal cells in vitro and in vivo. We present new evidence that nSMase2 deficiency results in shortening of motile cilia in the ependyma, suggesting that reduction of ceramide generation leads to ciliary dysregulation in vivo. Although it has not been described that mutations of enzymes in ceramide metabolism are linked to ciliopathies, our study shows that (phyto)ceramide levels and composition are important for adjusting cilium length. Therefore (phyto)ceramide is the first signaling sphingolipid demonstrated to metabolically regulate ciliogenesis by an evolutionarily conserved mechanism in *Chlamydomonas* and mammalian cells.

MATERIALS AND METHODS

Cultivation of *Chlamydomonas* and ependymal cells

All experiments were carried out according to an Animal Use Protocol approved by the Institutional Animal Care and Use Committee at Georgia Regents University. *Chlamydomonas reinhardtii* (wild-type strain CC-125 obtained from the *Chlamydomonas* Resource Center at the University of Minnesota, St. Paul, MN) was grown in Tris-acetate-phosphate (TAP) growth medium (Cellgro, Manassas, VA) in six-well plates or 250-ml Erlenmeyer flasks with a light/dark cycle of 14:10 h at room temperature. Primary cell culture of mixed glial cells was isolated from brains of 1-d-old C57BL/6 wild-type mouse pups. Brains were dissociated in phosphate-buffered saline (PBS) containing 0.1 M glucose, passed through a 40-μm filter, and plated in T-25 flasks in DMEM (Life Technologies, Grand Island, NY) supplemented with 10% fetal bovine serum and 1% penicillin/streptomycin solution at 37°C in a humidified atmosphere containing 5% CO_2. After 7 d, cells were passed to 24-well plates with poly-D-lysine–coated glass coverslips, and medium was changed to MEMα (Life Technologies) supplemented with bovine serum albumin (BSA; 0.5 mg/ml), insulin (10 μg/ml; bovine), transferrin (5.5 μg/ml), sodium selenite (6.7 ng/ml), and human thrombin (1 U/ml) to enrich for ependymal cells (Weibel *et al.*, 1986). Cultures of >70% proportion of ependymal cells were visible after another 7 d of cultivation in the thrombin-supplemented medium (purity was checked by immunocytochemistry for multiple versus primary cilia and glial markers such as glial fibrillary acid protein). Ependymal cells were treated with myriocin (Cayman, Ann Arbor, MI), GW4869 (Cayman), FB1 (Enzo Life Sciences, Farmingdale, NY), BIO (Sigma-Aldrich, St. Louis, MO), LiCl (Sigma-Aldrich), myristolyated pseudosubstrate (amino acids 113–125) inhibitor of PKCζ (PZI; Biomol, Plymouth Meeting, PA), and dihydrosphingosine (Avanti Polar Lipids, Alabaster, AL) at various concentrations and time periods in TAP or ependymal cell medium as indicated in *Results*.

Lipid analysis

Electrospray ionization/MS/MS analysis of endogenous (phyto)ceramide species was performed on a Thermo Fisher (Waltham, MA) Quantum triple quadrupole mass spectrometer operating in a Multiple Reaction Monitoring positive ionization mode, using modified a version (Bielawski *et al.*, 2006). Briefly, all biological materials were fortified with the internal standards (C_{17} base D-*erythro*-sphingosine [17CSph], C_{17} sphingosine-1-phosphate [17CSph-1P], *N*-palmitoyl-D-*erythro*-C_{13} sphingosine [13C16-Cer], and heptadecanoyl-D-*erythro*-sphingosine [C17-Cer] and C6-phytoceramide) and then extracted with ethyl acetate/isopropanol/water (60/30/10% vol/vol) solvent system. After evaporation and reconstitution in 150 μl of methanol, samples were injected on the HP1100/TSQ Quantum LC/MS system and gradient eluted from the BDS Hypersil C8, 150 × 3.2 mm, 3-μm–particle size column with 1.0 mM methanolic ammonium formate/2 mM aqueous ammonium formate mobile-phase system. Peaks corresponding to the target analytes and internal standards were collected and processed using the Xcalibur software system. Quantitative analysis was based on the calibration curves generated by spiking an artificial matrix with known amounts of the target analyte synthetic standards and an equal amount of internal standards (ISs). The target analyte/IS peak-area ratios were plotted against analyte concentration. The target analyte/IS peak-area ratios from the samples were similarly normalized to their respective ISs and compared with the calibration curves using a linear regression model. Introduction of the internal standards to the samples before extraction yields results already "recovery corrected," and therefore no further data manipulation is necessary.

RT-PCR

Total RNA was prepared from each experimental group of cells using TRIzol reagent following the manufacturer's protocol (Invitrogen/Life Technologies). First-strand cDNA was synthesized using an iScript cDNA Synthesis kit according to the manufacturer's instructions (Bio-Rad, Hercules, CA). GI:158275604 and GI:158278434 were used to design *Chlamydomonas* serine palmitoyltransferase 1 and 2 primers, respectively. GI:159490045 and GI:159465562 were used to design *Chlamydomonas* lag 1 and 2 primers, respectively. The following primers were used for RT-PCR:

mSPT1 (sense): 5′-TCCCTCCAGTCTCCAAGAAC-3′
mSPT1 (antisense): 5′-CAGGCTCTCCTCCAGGAATA-3′
mSPT2 (sense): 5′-CCACCATGCAACAGAAAGAG-3′
mSPT2 (antisense): 5′-AGGTTTCCAATTTCCTGACG-3′
ChlamySPT1 (sense): 5′-CCTGGCTTCCTACAACTACCTG-3′
ChlamySPT1 (antisense): 5′-CAAACGACTTGGTGAACGTG-3′
ChlamySPT2 (sense): 5′-CTGGAGGCGGAGGAGAAG-3′
ChlamySPT2 (antisense): 5′-CGAGGCGGAGAAGCAGTAG-3′
Chlamylag1 (sense): 5′-GTCGCACACCACATCGTCACC-3′
Chlamylag1 (antisense): 5′-GCAATCTCCACAATCTTGTAG-3′
Chlamylag2 (sense): 5′-TCTGCCGGGTCTGCTGGACAC-3′
Chlamylag2 (antisense): 5′-ATTGACGATGCCGAATGTGAG-3′

Deflagellation and reflagellation

Chlamydomonas cells were deflagellated in 10 mM 4-(2-hydroxyethyl)-1-piperazineethanesulfonic acid by lowering the pH to 4.5 with acetic acid for 60 s. The pH was rapidly neutralized by the addition of sodium hydroxide, and cells were transferred to TAP medium for further incubation in the presence or absence of myriocin (Wilson and Lefebvre, 2004).

Phototaxis motility assay

To analyze phototaxis behavior, *Chlamydomonas* was cultivated at a density of logarithmic growth rate and then transferred to a six-well dish. The wells were shielded from light in such a way that cells were only exposed to light coming from one defined direction. Cells with intact motility move toward and accumulate at the side exposed to light for 15–20 min. Phototaxis was quantified both by counting cells with a hemocytometer and by measuring optical absorbance of chlorophyll at 450 nm. All phototaxis experiments were performed 4 h after the beginning of the light phase (Lechtreck *et al.*, 2009).

Immunocytochemistry

Chlamydomonas or ependymal cells were grown in suspension or adherent on glass coverslips, respectively. Cells were fixed with 4% paraformaldehyde (PFA)/PBS for 15 min and then permeabilized by incubation with 0.2% Triton X-100 in PBS for 10 min at room temperature. Nonspecific binding sites were blocked with 3% ovalbumin/10% donkey serum/PBS for 1 h at 37°C. Primary antibodies used were as follows: anti–acetylated tubulin mouse IgG (1:3000; clone 6-1113-1, T6793; Sigma-Aldrich), anti-ceramide rabbit IgG (1:100, our laboratory; Krishnamurthy *et al.*, 2007a; He *et al.*, 2014), anti-ceramide mouse IgM (1:100, MAS0014; Glycobiotech, Kuekels, Germany), anti–pY216-GSK-3β rabbit IgG, anti–pY16-GSK-3β goat IgG, and anti–total GSK-3α/β mouse IgG (1:100; sc-135653, sc-11758, sc-7291; Santa Cruz Biotechnology, Dallas, TX), anti–pSer9-GSK-3β rabbit IgG (1:100; 9336S; Cell Signaling Technology, Beverly, MA), and anti-SPT2 antibody (1:1000; 10005260; Cayman). Secondary antibodies (Alexa Fluor 546–conjugated donkey anti-rabbit IgG, Cy5-conjugated donkey anti-mouse IgM, and μ-chain–specific, Alexa Fluor 647–conjugated goat anti-mouse IgG γ-chain specific; all Jackson ImmunoResearch, West Grove, PA) were diluted 1:300 in 0.1% ovalbumin/PBS and samples incubated for 2 h at 37°C. After washing, coverslips were mounted using Fluoroshield supplemented with 4′,6-diamidino-2-phenylindole (DAPI; Sigma-Aldrich) to visualize the nuclei. Confocal fluorescence microscopy was performed using a Zeiss LSM780 upright confocal laser scanning microscope (Zeiss, Jena, Germany) equipped with a two-photon argon laser at 488, 543, or 633 nm (Alexa Fluor 647), respectively. LSM 510 Meta 3.2 software was used for image acquisition. Images obtained with secondary antibody only were used as negative controls representing the background intensity in a particular laser channel.

Bifunctional ceramide analogue (pacFACer) cross-linking and conjugation with fluorophore

Chlamydomonas or ependymal cells were incubated under protection from light for 1 h in TAP medium or serum-free MEMα supplemented with vehicle (DMSO) or 5 μM bifunctional ceramide analogue *N*-(9-(3-pent-4-ynyl-3-H-diazirine-3-yl)-nonanoyl)-D-*erythro*-sphingosine (pacFACer; Avanti Polar Lipids) diluted 1:1000 from a stock in ethanol/2% dodecane. Cells were UV irradiated at 365 nm for 5 min at room temperature and fixed with 4% PFA/PBS for 15 min. Unbound pacFACer was removed by washing in methanol, methanol/chloroform (1:1), and methanol again for 5 min each. Cells were equilibrated in PBS and the click reaction performed using the Click-iT Cell Reaction Buffer Kit with Alexa Fluor 594 azide as the fluorophore following the manufacturer's protocol (Life Technologies).

Ceramide (lipid) ELISA and binding to aPKCζ and GSK-3β

Binding assays were performed using a modified lipid (ceramide) ELISA as described previously (Krishnamurthy *et al.*, 2007a; He *et al.*, 2014; Dinkins *et al.*, 2015). In brief, ceramides or pacFACer (500 ng in 50 μl of ethanol) were coated on 96-well Immulon-1B ELISA plates (Thermo Scientific/Life Technologies) and washed with PBS. Nonspecific binding sites were blocked by incubation for 1 h at 37°C with 200 μl of 1% fraction V BSA in PBS. Recombinant human aPKCζ (50 ng/50 μl; Enzo Life Sciences) or recombinant human GSK-3β (50 ng/50 μl; SignalChem, Richmond, Canada) in 0.1% BSA/PBS was incubated for 2 h at 37°C. Wells were washed three times with PBS and then incubated with 50 μl of 1:1000 α-PKCζ rabbit IgG (C20; sc-216; Santa Cruz Biotechnology) or 1:500 α-GSK-3α/β mouse IgG (sc-7291; Santa Cruz Biotechnology) overnight at 4°C. Wells were washed four times with PBS, incubated with secondary antibody (50 μl of 1:2000 α-rabbit IgG horseradish peroxidase (HRP) conjugated in 0.1% BSA/PBS; Jackson ImmunoResearch) for 2 h at 37°C, washed four times with PBS, and then developed using 0.8 mg/ml *o*-phenylenediamine and 0.03% hydrogen peroxide. After the reaction was stopped with 1 M sulfuric acid, optical absorbance was monitored at 492 nm.

Miscellaneous

For immunoblot analysis, protein concentrations were determined using the RC/DC protein assay, in accordance with the manufacturer's instructions (Bio-Rad). Equal amounts of protein were loaded onto a 4–20% gradient gel, and SDS–PAGE was performed using the Laemmli method. Ponceau S staining was performed to confirm equal loading. For immunoblotting, membranes were first blocked with 5% dry milk (or 3% BSA for phosphorylated proteins) in PBST (PBS containing 0.1% Tween-20) and incubated with primary antibodies SPT1/LCB1 antibody (1:1000; BD Transduction Laboratories, Franklin Lakes, NJ), SPT2 antibody (1:1000; Cayman), acetylated tubulin (1:10,000; Sigma-Aldrich,), total GSK-3α/β (1:500, Santa Cruz Biotechnology), pY216-GSK-3β (1:500; Santa Cruz Biotechnology), and pS9-GSK-3β (1:500; Cell Signaling) diluted in the blocking buffer overnight at 4°C. Membranes were then washed three times with PBST and incubated with the appropriate HRP-conjugated secondary antibodies (1:10,000; Jackson ImmunoResearch) for 1 h at room temperature. After washing, bands were detected using chemiluminescence reagent and exposure to x-ray film. Membranes were then stripped and reprobed, as described, with anti–β-actin (1:2000) to confirm equal loading.

Statistics

The mean, SEM, and statistical tests of control and treatment samples were calculated using GraphPad Prism (GraphPad, La Jolla, CA). We used Student's *t* test to compare two groups, one-way analysis of variance (ANOVA) with Bonferroni post hoc test for three or more groups, and nonlinear regression for motility assay (Figure 3B). Values of at least $p < 0.05$ were considered significant.

ACKNOWLEDGMENTS

We thank Christopher Poirier for providing the *fro/fro* mouse and Matt Laudon, curator at the *Chlamydomonas* Resource Center at the University of Minnesota, St. Paul, MN. This study was supported by grants to E.B. (National Science Foundation 1121579 and National Institutes of Health/National Institute on Aging 1R01AG03438) and M.D. (National Institutes of Health/National Institute on Aging 5 F32 AG044954-02). We are grateful for the support of the Imaging Core Facility at Georgia Regents University (under the supervision of Paul and Ana McNeil) and of the Department of Neuroscience and Regenerative Medicine (Chair, Lin Mei), Georgia Regents University.

REFERENCES

Bartke N, Hannun YA (2009). Bioactive sphingolipids: metabolism and function. J Lipid Res 50 (Suppl), S91–S96.

Berman SA, Wilson NF, Haas NA, Lefebvre PA (2003). A novel MAP kinase regulates flagellar length in Chlamydomonas. Curr Biol 13, 1145–1149.

Beurel E, Grieco SF, Jope RS (2015). Glycogen synthase kinase-3 (GSK3): regulation, actions, and diseases. Pharmacol Ther 148, 114–131.

Bieberich E (2011). Ceramide in stem cell differentiation and embryo development: novel functions of a topological cell-signaling lipid and the concept of ceramide compartments. J Lipids 2011, 610306.

Bieberich E (2012). It's a lipid's world: bioactive lipid metabolism and signaling in neural stem cell differentiation. Neurochem Res 37, 1208–1229.

Bieberich E, Kawaguchi T, Yu RK (2000). N-acylated serinol is a novel ceramide mimic inducing apoptosis in neuroblastoma cells. J Biol Chem 275, 177–181.
Bielawski J, Szulc ZM, Hannun YA, Bielawska A (2006). Simultaneous quantitative analysis of bioactive sphingolipids by high-performance liquid chromatography-tandem mass spectrometry. Methods 39, 82–91.
Bourbon NA, Yun J, Kester M (2000). Ceramide directly activates protein kinase C zeta to regulate a stress-activated protein kinase signaling complex. J Biol Chem 275, 35617–35623.
Broekhuis JR, Verhey KJ, Jansen G (2014). Regulation of cilium length and intraflagellar transport by the RCK-kinases ICK and MOK in renal epithelial cells. PLoS One 9, e108470.
Cao M, Li G, Pan J (2009). Regulation of cilia assembly, disassembly, and length by protein phosphorylation. Methods Cell Biol 94, 333–346.
Cao M, Meng D, Wang L, Bei S, Snell WJ, Pan J (2013). Activation loop phosphorylation of a protein kinase is a molecular marker of organelle size that dynamically reports flagellar length. Proc Natl Acad Sci USA 110, 12337–12342.
Dasgupta S, Kong J, Bieberich E (2013). Phytoceramide in vertebrate tissues: one step chromatography separation for molecular characterization of ceramide species. PLoS One 8, e80841.
Dinkins MB, Dasgupta S, Wang G, Zhu G, He Q, Kong JN, Bieberich E (2015). The 5XFAD mouse model of alzheimer's disease exhibits an age-dependent increase in anti-ceramide IgG and exogenous administration of ceramide further increases anti-ceramide titers and amyloid plaque burden. J Alzheimers Dis 46, 55–61.
Etienne-Manneville S, Hall A (2003). Cdc42 regulates GSK-3beta and adenomatous polyposis coli to control cell polarity. Nature 421, 753–756.
Fan S, Hurd TW, Liu CJ, Straight SW, Weimbs T, Hurd EA, Domino SE, Margolis B (2004). Polarity proteins control ciliogenesis via kinesin motor interactions. Curr Biol 14, 1451–1461.
Fox TE, Houck KL, O'Neill SM, Nagarajan M, Stover TC, Pomianowski PT, Unal O, Yun JK, Naides SJ, Kester M (2007). Ceramide recruits and activates protein kinase C zeta (PKC zeta) within structured membrane microdomains. J Biol Chem 282, 12450–12457.
Gault CR, Obeid LM, Hannun YA (2010). An overview of sphingolipid metabolism: from synthesis to breakdown. Adv Exp Med Biol 688, 1–23.
Goedhart J, Gadella TW Jr (2004). Photolysis of caged phosphatidic acid induces flagellar excision in Chlamydomonas. Biochemistry 43, 4263–4271.
Guenet JL, Stanescu R, Maroteaux P, Stanescu V (1981). Fragilitas ossium: a new autosomal recessive mutation in the mouse. J Hered 72, 440–441.
Hanada K, Nishijima M, Fujita T, Kobayashi S (2000). Specificity of inhibitors of serine palmitoyltransferase (SPT), a key enzyme in sphingolipid biosynthesis, in intact cells. A novel evaluation system using an SPT-defective mammalian cell mutant. Biochem Pharmacol 59, 1211–1216.
Hannun YA (1996). Functions of ceramide in coordinating cellular responses to stress. Science 274, 1855–1859.
Hannun YA, Obeid LM (2011). Many ceramides. J Biol Chem 286, 27855–27862.
He Q, Wang G, Dasgupta S, Dinkins M, Zhu G, Bieberich E (2012). Characterization of an apical ceramide-enriched compartment regulating ciliogenesis. Mol Biol Cell 23, 3156–3166.
He Q, Wang G, Wakade S, Dasgupta S, Dinkins M, Kong JN, Spassieva SD, Bieberich E (2014). Primary cilia in stem cells and neural progenitors are regulated by neutral sphingomyelinase 2 and ceramide. Mol Biol Cell 25, 1715–1729.
Hilton LK, Gunawardane K, Kim JW, Schwarz MC, Quarmby LM (2013). The kinases LF4 and CNK2 control ciliary length by feedback regulation of assembly and disassembly rates. Curr Biol 23, 2208–2214.
Kim M, Datta A, Brakeman P, Yu W, Mostov KE (2007). Polarity proteins PAR6 and aPKC regulate cell death through GSK-3beta in 3D epithelial morphogenesis. J Cell Sci 120, 2309–2317.
Krishnamurthy K, Dasgupta S, Bieberich E (2007a). Development and characterization of a novel anti-ceramide antibody. J Lipid Res 48, 968–975.
Krishnamurthy K, Wang G, Silva J, Condie BG, Bieberich E (2007b). Ceramide regulates atypical pkczeta/lambda-mediated cell polarity in primitive ectoderm cells: a novel function of sphingolipids in morphogenesis. J Biol Chem 282, 3379–3390.
Kruse M, Gamulin V, Cetkovic H, Pancer Z, Muller IM, Muller WE (1996). Molecular evolution of the metazoan protein kinase C multigene family. J Mol Evol 43, 374–383.
Lechtreck KF, Brown JM, Sampaio JL, Craft JM, Shevchenko A, Evans JE, Witman GB (2013). Cycling of the signaling protein phospholipase D through cilia requires the BBSome only for the export phase. J Cell Biol 201, 249–261.
Lechtreck KF, Johnson EC, Sakai T, Cochran D, Ballif BA, Rush J, Pazour GJ, Ikebe M, Witman GB (2009). The Chlamydomonas reinhardtii BBSome is an IFT cargo required for export of specific signaling proteins from flagella. J Cell Biol 187, 1117–1132.
Lester RL, Dickson RC (1993). Sphingolipids with inositolphosphate-containing head groups. Adv Lipid Res 26, 253–274.
Loktev AV, Zhang Q, Beck JS, Searby CC, Scheetz TE, Bazan JF, Slusarski DC, Sheffield VC, Jackson PK, Nachury MV (2008). A BBSome subunit links ciliogenesis, microtubule stability, and acetylation. Dev Cell 15, 854–865.
Lozano J, Berra E, Municio MM, Diaz-Meco MT, Dominguez I, Sanz L, Moscat J (1994). Protein kinase C zeta isoform is critical for kappa B-dependent promoter activation by sphingomyelinase. J Biol Chem 269, 19200–19202.
Markham JE, Lynch DV, Napier JA, Dunn TM, Cahoon EB (2013). Plant sphingolipids: function follows form. Curr Opin Plant Biol 16, 350–357.
Maruta H, Greer K, Rosenbaum JL (1986). The acetylation of alpha-tubulin and its relationship to the assembly and disassembly of microtubules. J Cell Biol 103, 571–579.
Milhas D, Clarke CJ, Hannun YA (2010). Sphingomyelin metabolism at the plasma membrane: implications for bioactive sphingolipids. FEBS Lett 584, 1887–1894.
Miyake Y, Kozutsumi Y, Nakamura S, Fujita T, Kawasaki T (1995). Serine palmitoyltransferase is the primary target of a sphingosine-like immunosuppressant, ISP-1/myriocin. Biochem Biophys Res Commun 211, 396–403.
Muller G, Ayoub M, Storz P, Rennecke J, Fabbro D, Pfizenmaier K (1995). PKC zeta is a molecular switch in signal transduction of TNF-alpha, bifunctionally regulated by ceramide and arachidonic acid. EMBO J 14, 1961–1969.
Muscoli C, Doyle T, Dagostino C, Bryant L, Chen Z, Watkins LR, Ryerse J, Bieberich E, Neumman W, Salvemini D (2010). Counter-regulation of opioid analgesia by glial-derived bioactive sphingolipids. J Neurosci 30, 15400–15408.
Nakakura T, Asano-Hoshino A, Suzuki T, Arisawa K, Tanaka H, Sekino Y, Kiuchi Y, Kawai K, Hagiwara H (2014). The elongation of primary cilia via the acetylation of alpha-tubulin by the treatment with lithium chloride in human fibroblast KD cells. Med Mol Morphol 48, 44–53.
Nikolova-Karakashian M, Karakashian A, Rutkute K (2008). Role of neutral sphingomyelinases in aging and inflammation. Subcell Biochem 49, 469–486.
Ossipova O, Tabler J, Green JB, Sokol SY (2007). PAR1 specifies ciliated cells in vertebrate ectoderm downstream of aPKC. Development 134, 4297–4306.
Ou Y, Ruan Y, Cheng M, Moser JJ, Rattner JB, van der Hoorn FA (2009). Adenylate cyclase regulates elongation of mammalian primary cilia. Exp Cell Res 315, 2802–2817.
Pan J, Wang Q, Snell WJ (2004). An aurora kinase is essential for flagellar disassembly in Chlamydomonas. Dev Cell 6, 445–451.
Pata MO, Hannun YA, Ng CK (2010). Plant sphingolipids: decoding the enigma of the Sphinx. New Phytol 185, 611–630.
Poirier C, Berdyshev EV, Dimitropoulou C, Bogatcheva NV, Biddinger PW, Verin AD (2012). Neutral sphingomyelinase 2 deficiency is associated with lung anomalies similar to emphysema. Mamm Genome 23, 758–763.
Pruliere G, Cosson J, Chevalier S, Sardet C, Chenevert J (2011). Atypical protein kinase C controls sea urchin ciliogenesis. Mol Biol Cell 22, 2042–2053.
Pugacheva EN, Jablonski SA, Hartman TR, Henske EP, Golemis EA (2007). HEF1-dependent Aurora A activation induces disassembly of the primary cilium. Cell 129, 1351–1363.
Quarmby LM, Yueh YG, Cheshire JL, Keller LR, Snell WJ, Crain RC (1992). Inositol phospholipid metabolism may trigger flagellar excision in Chlamydomonas reinhardtii. J Cell Biol 116, 737–744.
Satir P, Pedersen LB, Christensen ST (2010). The primary cilium at a glance. J Cell Sci 123, 499–503.
Sato N, Meijer L, Skaltsounis L, Greengard P, Brivanlou AH (2004). Maintenance of pluripotency in human and mouse embryonic stem cells through activation of Wnt signaling by a pharmacological GSK-3-specific inhibitor. Nat Med 10, 55–63.
Shamseddine AA, Airola MV, Hannun YA (2015). Roles and regulation of neutral sphingomyelinase-2 in cellular and pathological processes. Adv Biol Regul 57, 24–41.
Silflow CD, Lefebvre PA (2001). Assembly and motility of eukaryotic cilia and flagella. Lessons from Chlamydomonas reinhardtii. Plant Physiol 127, 1500–1507.

Snell WJ, Pan J, Wang Q (2004). Cilia and flagella revealed: from flagellar assembly in Chlamydomonas to human obesity disorders. Cell 117, 693–697.
Song L, Jia Y, Zhu W, Newton IP, Li Z, Li W (2014). N-terminal truncation mutations of adenomatous polyposis coli are associated with primary cilia defects. Int J Biochem Cell Biol 55C, 79–86.
Spassieva SD, Markham JE, Hille J (2002). The plant disease resistance gene Asc-1 prevents disruption of sphingolipid metabolism during AAL-toxin-induced programmed cell death. Plant J 32, 561–572.
Sperling P, Heinz E (2003). Plant sphingolipids: structural diversity, biosynthesis, first genes and functions. Biochim Biophys Acta 1632, 1–15.
Sung CH, Leroux MR (2013). The roles of evolutionarily conserved functional modules in cilia-related trafficking. Nat Cell Biol 15, 1387–1397.
Szebenyi G, Morfini G, Brady ST (2002). Pictures in cell biology. GSK-3 and regulation of kinesin function. Trends Cell Biol 12, 245.
Thoma CR, Frew IJ, Hoerner CR, Montani M, Moch H, Krek W (2007). pVHL and GSK3beta are components of a primary cilium-maintenance signalling network. Nat Cell Biol 9, 588–595.
Vincensini L, Blisnick T, Bastin P (2011). 1001 model organisms to study cilia and flagella. Biol Cell 103, 109–130.
Wadsworth JM, Clarke DJ, McMahon SA, Lowther JP, Beattie AE, Langridge-Smith PR, Broughton HB, Dunn TM, Naismith JH, Campopiano DJ (2013). The chemical basis of serine palmitoyltransferase inhibition by myriocin. J Am Chem Soc 135, 14276–14285.
Wang E, Norred WP, Bacon CW, Riley RT, Merrill AH Jr (1991). Inhibition of sphingolipid biosynthesis by fumonisins. Implications for diseases associated with Fusarium moniliforme. J Biol Chem 266, 14486–14490.
Wang G, Dinkins M, He Q, Zhu G, Poirier C, Campbell A, Mayer-Proschel M, Bieberich E (2012). Astrocytes secrete exosomes enriched with proapoptotic ceramide and prostate apoptosis response 4 (PAR-4): potential mechanism of apoptosis induction in Alzheimer disease (AD). J Biol Chem 287, 21384–21395.
Wang G, Krishnamurthy K, Bieberich E (2009a). Regulation of primary cilia formation by ceramide. J Lipid Res 50, 2103–2110.
Wang G, Krishnamurthy K, Umapathy NS, Verin AD, Bieberich E (2009b). The carboxyl-terminal domain of atypical protein kinase Czeta binds to ceramide and regulates junction formation in epithelial cells. J Biol Chem 284, 14469–14475.
Wang G, Silva J, Krishnamurthy K, Tran E, Condie BG, Bieberich E (2005). Direct binding to ceramide activates protein kinase Czeta before the formation of a pro-apoptotic complex with PAR-4 in differentiating stem cells. J Biol Chem 280, 26415–26424.
Wang YM, Seibenhener ML, Vandenplas ML, Wooten MW (1999). Atypical PKC zeta is activated by ceramide, resulting in coactivation of NF-kappaB/JNK kinase and cell survival. J Neurosci Res 55, 293–302.
Weibel M, Pettmann B, Artault JC, Sensenbrenner M, Labourdette G (1986). Primary culture of rat ependymal cells in serum-free defined medium. Brain Res 390, 199–209.
Wilson NF, Lefebvre PA (2004). Regulation of flagellar assembly by glycogen synthase kinase 3 in Chlamydomonas reinhardtii. Eukaryot Cell 3, 1307–1319.
Young CC, van der Harg JM, Lewis NJ, Brooks KJ, Buchan AM, Szele FG (2013). Ependymal ciliary dysfunction and reactive astrocytosis in a reorganized subventricular zone after stroke. Cereb Cortex 23, 647–659.